IMPROVEMENT OF THE PLASMA-WALL MODEL ON A FLUID-PIC CODE OF A HALL THRUSTER

Félix I. Parra[1], Eduardo Ahedo[1], Manuel Martínez-Sánchez[2], and John Michael Fife[3]

[1]E.T.S.I. Aeronáuticos, Universidad Politécnica, 28040 Madrid, Spain
[2]Massachusetts Institute of Technology, Cambridge, USA
[3]Air Force Research Laboratory, Edwards AFB, California, USA

ABSTRACT

Two issues are discussed. First, a new sheath model that takes into account charge-saturation is implemented in HPHall. Second, the transition between the quasineutral solution and the sheaths at the lateral walls is found to be treated deficiently in the original code. The use of finer meshes yields better solutions but do not solve the problem completely.

Key words: Hall thrusters; particle-in-cell codes; sheaths.

1. INTRODUCTION

The HPHall hybrid code started to be developed ten years ago (Fife & Martínez-Sánchez 1995; Fife 1998). HPHall analyzes the two-dimensional (2D) (azimuthal symmetry is assumed) structure of the plasma discharge in a Hall thruster chamber by treating (i) ions and neutrals with particle-in-cell(PIC) plus Montecarlo methods and (ii) electrons with macroscopic equations. Hybrid codes represents a good trade-off between fully macroscopic and fully PIC codes if we take into account (a) the disparate length and time scales of electrons and heavy species, (b) the treatment of complex geometries and magnetic field topographies, and (b) the execution time.

The HPHall has been proved very helpful in the analysis of the response of the SPT-70 and other Hall thrusters. Nonetheless, in order to deliver a valid first version of the code within a reasonable time, some parts of it were deliberately underdeveloped. In addition, important advances on the understanding of the multiple discharge phenomena have been made in the last years, and better or new models of these phenomena are available today. All this has motivated to launch a program to improve (i) the numerical tools and outputs of HPHall and (ii) the underlying physics implemented on it. A lateral goal of the program is the comparison and mutual validation of HPHall and the macroscopic code developed by Ahedo et al. (2003).

In this paper, two specific subjects related to the plasma interaction with the lateral walls are discussed and improved:

1. Implementation of the charge-saturation sheath model developed by Ahedo (2002b).
2. Fulfillment of the Bohm condition at the plasma/sheath transition (Ahedo 2002a).

2. HPHALL FUNDAMENTALS

The reader is referred to Fife (1998) for a detailed account of HPHall. In particular, Fig. 3.9 of that work shows the code computation diagram. The geometric mesh and the magnetic field are obtained in a pre-process. Figure 1 shows the first ('coarse') mesh and the magnetic field used in the present work. Parameters correspond to a SPT-70 thruster. In order to better compare with the model of Ahedo et al., the B-field has been assumed to have no axial component ($B_z = 0$) so that B-lines are along the radial direction. For the radial component we take $B_r \propto 1/r$. In this way we are fulfilling $\nabla \cdot \boldsymbol{B} = 0$, but not $\nabla \wedge \boldsymbol{B} = \boldsymbol{0}$.

The PIC and fluid parts of the code are separated. The PIC algorithms yield the motion of ion and neutral macroparticles (about 60.000 and 30.000,

Proc. '4th Int. Spacecraft Propulsion Conference', Cagliari, Sardinia, Italy 2-4 June 2004 (ESA SP-555, October 2004)

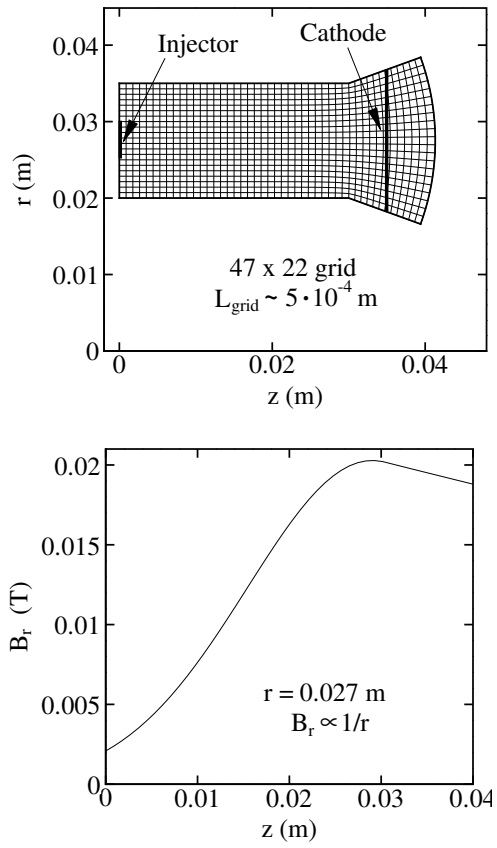

Figure 1. 'Coarse' mesh and B-field used in this work. For the magnetic field, one has $B_z = 0$ and $B_r(r,z) = B_r(r_0,z)r_0/r$.

respectively, for the above mesh). This motion is collisionless except for ionization (by electron-neutral impact) and recombination processes at the walls. These are treated with Montecarlo methods. Linear weighting is used to define macroscopic magnitudes (like densities, fluxes, and temperatures) at the mesh nodes.

Electrons dynamics are modelled by 2D macroscopic equations based on a closed-drift, diffusive model. The electron equations are solved by finite element methods. The strong magnetic field introduces a high anisotropy on the electron momentum equations, which leads to a Maxwell-Boltzmann equilibrium along the magnetic lines and a generalized Ohm law in the direction perpendicular to them. Then, the best volume elements to integrate the electron equations have the magnetic lines as boundaries.

The Hall thruster discharge is quasineutral except for very thin Debye sheaths tied to the lateral walls and the anode. The macroscopic modelling of the electrons dynamics makes possible to apply plasma quasineutrality within the code. This avoids to solve Poisson equation for the electrostatic potential, ϕ, and consequently to use the small time and length scales associated to that equation (i.e. the inverse of plasma frequency and the Debye length). This reduces largely the code execution time.

Because of quasineutrality, the plasma density, n_e, is determined by the PIC computations on the ions. Then, the Maxwell-Boltzmann equilibrium law relates n_e and the electron temperature, T_e, to the electrostatic potential. The electron energy equation, the Ohm law perpendicular to magnetic lines, and the electrical current conservation are needed to compute T_e. (This constitutes the main part of the electron-related part of the code.) The electric field is computed subsequently from $\boldsymbol{E} = -\nabla\phi$ and used in the next time step of the PIC code.

The main inconvenient of using quasineutrality is that the computation domain does not end at the thruster walls but at the transitions to the quasineutral sheaths. This means that (i) sheaths must be solved separately and (ii) wall conditions must be substituted by sheath transition conditions. We will see below that this last point is a rather problematic issue in HPHall.

3. PLASMA-WALL INTERACTION FUNDAMENTALS

SPT discharge chambers use ceramic materials. The behavior of the plasma in their vicinity defines the particle and energy losses to them, so a correct modelling is necessary for a valid simulation. In this section we resume the basic features of the plasma-wall interaction as were established recently by Ahedo (2002a,b).

For a dielectric material, the plasma structure near the wall is a consequence of the local zero-current condition. The disparate electron and ion random fluxes make impossible to satisfy that condition by the quasineutral plasma so a non-neutral sheath is formed, Fig. 2. In a two-scale asymptotic analysis, based on (Debye length) $\ll$ (channel width), the plasma sheath transition (point Q) is *perfectly defined* and the quasineutral and sheath regions are solved independently. The sheath is planar and collisionless, and the sheath potential drop, ϕ_{WQ}, is self-adjusted in order to satisfy the zero-current condition. The analyses of the quasineutral and sheath regions demonstrate that the transition between the two regions is possible only if the plasma satisfies the (sonic) Bohm condition. The functional form of this condition depends on the particular plasma characteristics. For a simple two

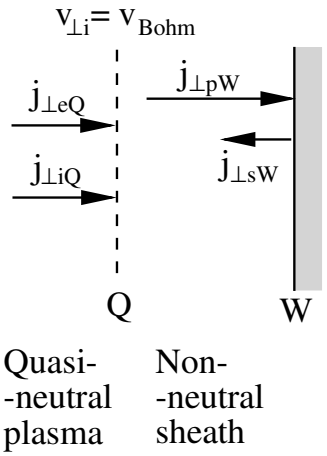

Figure 2. Sketch of the presheath/sheath model. Q is the sheath transition, and W is the wall. p and s represent primary and secondary electrons in the sheath. e represents electrons in the presheath. $j_\perp$ are currents perpendicular to the wall.

species plasma, the Bohm condition states that the ion (macroscopic) velocity perpendicular to the wall (and sheath) is sonic,

$$v_{\perp iQ} = v_{Bohm} = \sqrt{\frac{kT_{eQ} + kT_{iQ}}{m_i}}. \qquad (1)$$

For dielectric materials, such as Boron Nitride composites used in Hall thrusters, secondary electron emission (SEE) by electron impact is high. SEE can modify largely the sheath structure (Hobbs & Wesson 1967). The account for SEE within a consistent sheath/presheath/sheath model for a plasma flowing between two walls was achieved by Ahedo (2002b). A central idea of the model was to distinguish between primary (p) and secondary (s) electrons within the sheath, but to consider a single electron population (e) in the quasineutral or presheath region. The temperatures of populations p and e in the model differ up to a 15% for high SEE. The presence of secondary electrons has a small impact within the presheath structure.

When SEE is present, the zero-current condition reads

$$\begin{aligned} g_{\perp iW} = g_{\perp iQ} = g_{\perp pW} + g_{\perp sW}, \\ g_{\perp sW} = -\delta_w(T_p) g_{\perp pW}, \end{aligned} \qquad (2)$$

where $g_\perp$ represent particle fluxes perpendicular to the walls, and $\delta_w(T_p)$ is the effective SEE yield, which depends, at least, on the temperature of primary electrons and the wall material. For a Maxwellian population, the primary flux is

$$g_{\perp pW} = n_{pQ} \exp\left(-\frac{e\phi_{WQ}}{kT_p}\right) \sqrt{\frac{kT_p}{2\pi m_e}} \qquad (3)$$

and applying Eq. (2) the sheath potential drop satisfies

$$\frac{e\phi_{WQ}}{kT_p} = \ln\sqrt{\frac{m_i}{2\pi m_e}} + \ln(1-\delta_w) + \ln\frac{n_{pQ}\sqrt{kT_p/m_i}}{n_{eQ} v_{\perp iQ}}; \qquad (4)$$

the first term on the right-hand side is 5.28, and the last term is practically zero, even for $\delta_w \sim 1$. As δ_w increases, $e\phi_{WQ}/kT_p$ decreases and the electric field at the wall decreases too. For $\delta_w = \delta_w^* = 0.983$ (and xenon), this electric field becomes zero, that is, the charge saturation limit (CSL) is reached. The potential drop in the CSL is $e\phi_{WQ}/kT_p \simeq 1.02$ and the p-e temperature ratio is $T_p/T_e \simeq 0.86$ (Ahedo 2002b). For higher values of δ_w we are within the charge saturation regime (CSR). A small potential well (of the order of the wall temperature, T_w) is formed in order to turn back part of the secondary emission. As a consequence, the secondary flux that crosses the sheath and reaches the presheath continues to be $j_{\perp sQ} = -\delta_w^* j_{\perp pW}$. If $T_w \ll T_p$, the potential well is negligible and the CSL dimensionless solution represents the whole CSR.

The electron energy flux into the wall is

$$q_{\perp pW} = g_{\perp pW} 2T_p = \frac{g_{\perp iQ}}{1-\delta_w} 2T_p \qquad (5)$$

For a quasineutral code, it is more important the electron energy flux into the sheath (at point Q):

$$q_{\perp eQ} = q_{\perp pQ} + q_{\perp sQ} = g_{\perp iQ}\left(\frac{2T_p}{1-\delta_w} + e\phi_{WQ}\right) \qquad (6)$$

Here the ion (and electron) flux into the sheath, $g_{\perp iQ}$, depends almost exclusively on the plasma evolution within the quasineutral region, whereas the energy losses per electron, $q_{\perp eQ}/g_{\perp iQ}$, depend on the sheath physics, that is on the SEE.

SEE depends on the specific material. In general the experimental data provides the SEE yield for a monoenergetic beam of energy E. At present, there are no accurate measurements of $\delta_w(E)$ for low beam energies. This justifies that existing models opt for either potential laws: $\delta_w(E) = (E/E_1)^B$, or linear laws, $\delta_w(E) = \delta_0 + (1-\delta_0)E/E_1$; in both cases E_1 is the energy for 100% SEE. Here, we will use the potential law implemented in the HPHall. For a Maxwellian distribution of primary electrons, the effective SEE yield is obtained from averaging

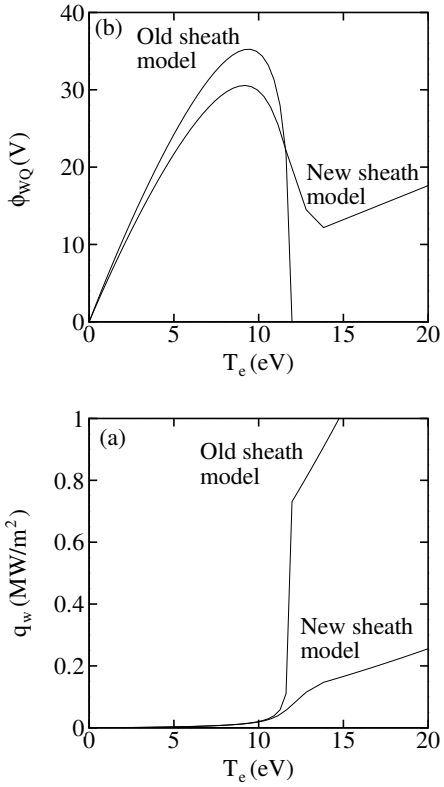

Figure 3. Comparison between the old and new sheath models for a ceramic material with $E_1 = 21.68$ eV and $B = 0.576$. (a) Sheath potential drop. (b) Electron energy flux into the sheath for $n_{eQ} = 2 \cdot 10^{17}$ m^{-3}.

$\delta_w(E)$ over the different energies. This yields (Fife et al. 1997)

$$\delta_w(T_p) = (T_p/T_1)^B, \qquad (7)$$

with $T_1 = E_1/\Gamma(2+B)^{1/B}$. For usual ceramics, it is $E_1 \sim 15 - 50$eV.

4. IMPLEMENTATION OF A NEW SHEATH MODEL

When HPHall was developed, the charge saturation of the sheath was unknown to researchers on Hall thruster physics. It was first noted to this community by Jolivet & Roussel (2000). Previous models (Morozov 1991; Fife et al. 1997) considered that the sheath vanishes for SEE yields close to 100%. In particular, in the model that was implemented in HPHall the electron-repelling sheath vanishes for $\delta_w \simeq 0.997$. No-sheath and ion-repelling sheath regimes follow for larger δ_w. Since $T_w \ll T_e$, the potential drop for the ion-repelling sheath can be neglected (but a Bohm condition on the attracted electron flux still applies). The sheath vanishing implies much larger electron fluxes to the wall, Eq. (3), and consequently, larger energy losses.

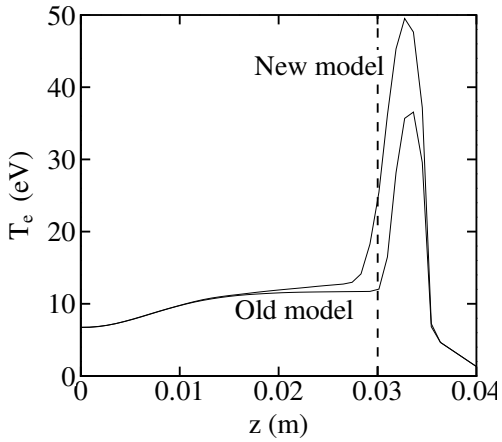

Figure 4. Temperature profiles along the chamber obtained from HPHall for $V_d = 600\,V$ and the two sheath models of Fig. 3.

Figure 3(a) compares, for a particular material, the original (old) sheath model of HPHall and the correct (new) one. Apart from the main difference (sheath charge-saturation versus sheath vanishing), the two models present some differences in the way they compute T_p and n_{eQ}. The character of the sheath changes at $T_e = 12.0$ eV for the old model, and at $T_e = 13.6$ eV ($T_p = 11.7$ eV) for the new model. Figure 3(b) compares the electron energy fluxes into the sheath for the two models. Notice that for high temperatures the energy losses are almost one order of magnitude larger in the old model.

The HPHall code has been run to compare the discharge response when the old and new sheath models are used. Figure 4 depicts the temperature profiles, $T_e(z)$, (T_e is constant radially) for a discharge voltage of 600 V (and parameters of Figs. 1 and 3). In both cases, high energy losses take place in a region near the chamber exit, due to either charge saturation or vanishing of the sheath, depending on the sheath model. The lower energy losses at the same temperature in the new model lead to a higher peak temperature, while the total energy lost into the walls remains similar in both models: 611 W in the old one versus 586 W in the new one. Heat conduction effects push the temperature peak outside the chamber exit. Notice that the temperature profile is practically the same with both models in the inner part of the chamber (that is for values of

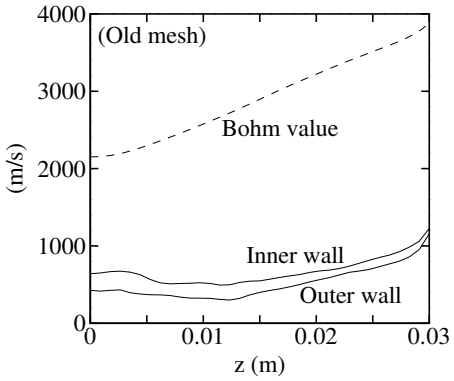

Figure 5. Ion perpendicular velocity at the lateral ends of the domain and the Bohm velocity, along the chamber.

T_e below 11 eV) where differences between the two models are not large. [This example with a high discharge voltage has been chosen to stand out the differences between the two models, and no attempt has been made to adjust parameters to obtain a solution with high efficiency.]

5. CORRECTION OF THE PLASMA/SHEATH TRANSITION

5.1. The sheath transition problem

Figure 5 plots the distribution of radial ion (macroscopic) velocities at the inner and outer boundaries of the mesh as computed by HPHall for the case of Fig. 1. These velocities are much lower than the Bohm velocity. Eq. (1). Therefore, the radial ends of the computational domain (point T hereafter) are not coinciding with the sheath transition point Q. The sheath equations do not admit a valid solution departing from $v_{\perp iT} < v_{Bohm}$. Since radial gradients become very large near point Q, Fife assumed (more or less explicitly) that the ion acceleration to the sonic value took place in a thin quasineutral layer TQ; formally, the thickness of this layer, l_{TQ}, must satisfy

$$\lambda_D \ll l_{TQ} \ll l_{cell}, \tag{8}$$

with l_{cell} the thickness of the cell contiguous to boundary T. Figure 6 sketches this 'virtual' layer. Then, assuming free ion acceleration across this layer and $v_{\perp iT} \ll v_{Bohm}$, the potential and density drops across layer TQ satisfy

$$\phi_{QT} = \frac{kT_e}{2e}, \qquad n_{eQ} = n_{eT}\exp(-1/2). \tag{9}$$

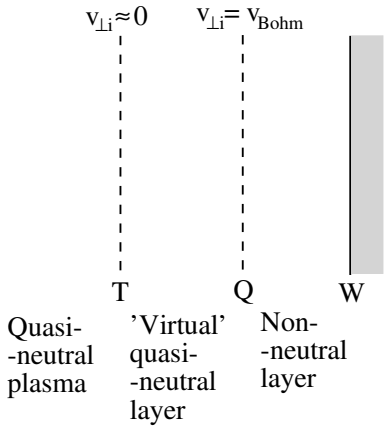

Figure 6. Sketch of HPHall sheath transition. T is the end of the computational domain.

HPHall uses these values to define the electron flux into the sheath (and the wall) as

$$g_{\perp eQ} = g_{Bohm} = n_{eT}\exp(-1/2)v_{Bohm}. \tag{10}$$

However, this procedure is inconsistent:

1. One has $g_{Bohm} > g_{\perp iT}$, so that a plasma production mechanism should exist in layer TQ to provide the increment of plasma flux. The layer is too thin for ionization to be significant there. Furthermore, it would be inconsistent to have large ionization in layer TQ whereas ionization has been found small along the rest of the chamber width.

2. The PIC code ignores the existence of any added layer TQ. Then the ion flux actually delivered into the wall is $g_{\perp iW} = g_{\perp iT}$ and plasma recombination is based on that value. Thus, the recombined neutral flux is $g_{\perp nW} = -g_{\perp iW}$, much smaller than the expected value. [Observe the feedback mechanism that keeps $g_{\perp iT}$ low: low neutral recombination density yields low ionization, which yields low radial ion fluxes, and so on.]

3. The electron code uses condition (10) so that the zero current condition is not satisfied.

Therefore, the invocation of an extra layer between the computational domain and the sheath seems very dubious. The PIC code should be able to provide the Bohm flux at the inner and outer radial boundaries (that is point T must coincide with point Q). Three ways are being envisaged to correct this problem:

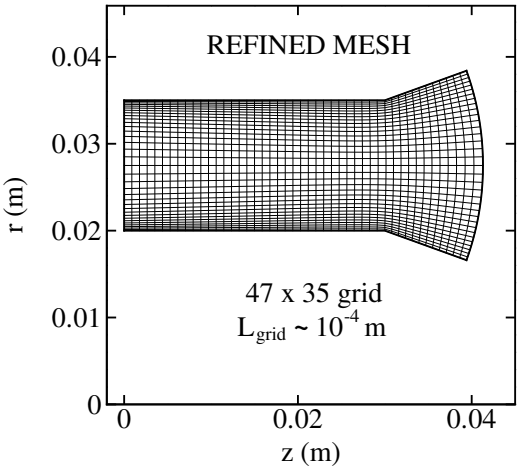

Figure 7. The refined mesh.

1. To use a refined mesh.
2. To modify the way ion magnitudes are weighed in the boundary nodes.
3. To implement somehow the (macroscopic) Bohm condition within the ion PIC code.

Here, only the first proposal is analyzed.

5.2. Solution with a refined mesh

A more refined mesh must provide more accurate results. In addition, it should give answers to two questions. The first one is whether the invocation of the above layer TQ has a physical sense. The second one is whether the PIC code tends to fulfill 'naturally' the Bohm condition at the radial boundaries (as it does happen, for instance, when it simulates a fluid discharge into the vacuum).

Figure 7 shows the new mesh we have used. The length of the cells close to the boundaries is five times less than in the old mesh. To maintain stability and statistical representativeness, the time step is divided by five and the particle number is multiplied by five. As a result, the execution time to obtain a stationary solution increases by about 20 times (from 50 minutes to 15 hours in a Pentium III 2.4 GHz).

Figure 8 shows radial profiles of several magnitudes at an intermediate axial position within the chamber, using the coarse and refined meshes. The comparison of results demonstrates that the radial structure varies significantly with the new mesh. Radial ion velocities and presheath potential drops

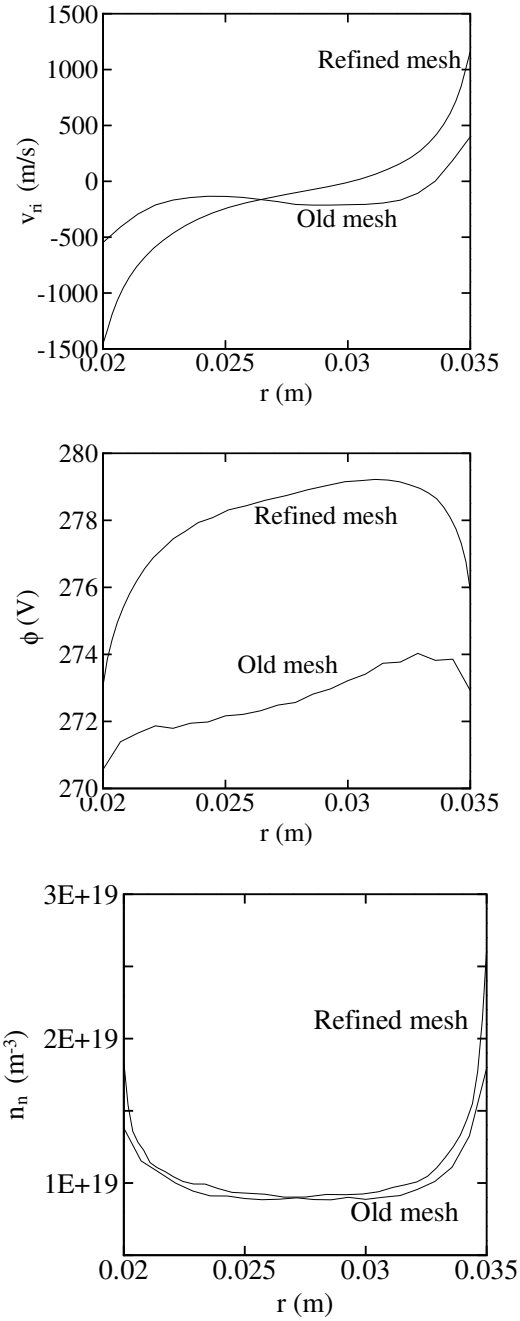

Figure 8. Radial profiles at $z = 0.015$ m.

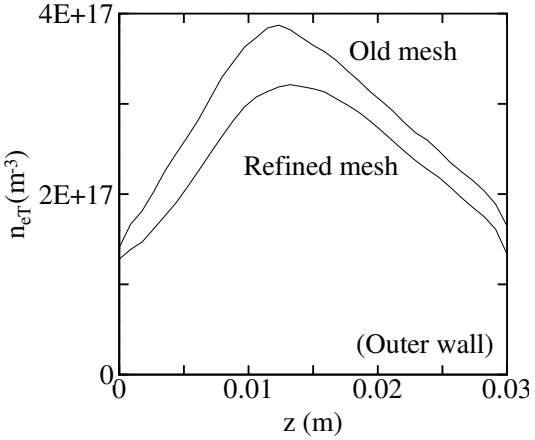

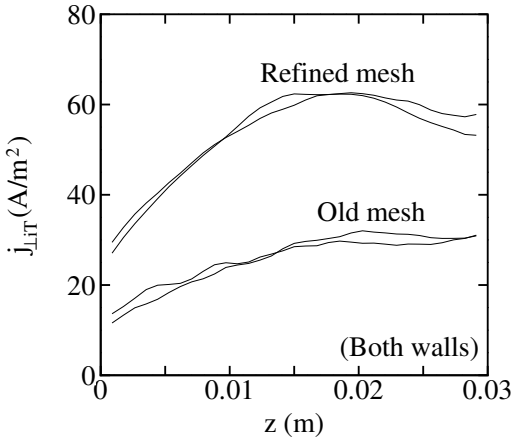

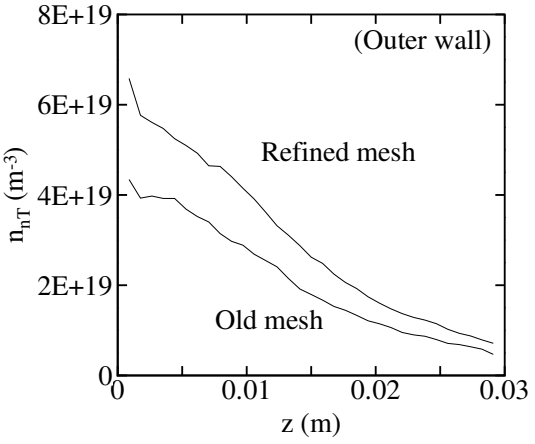

Figure 9. Axial profiles at the inner and outer boundaries for the old and refined meshes.

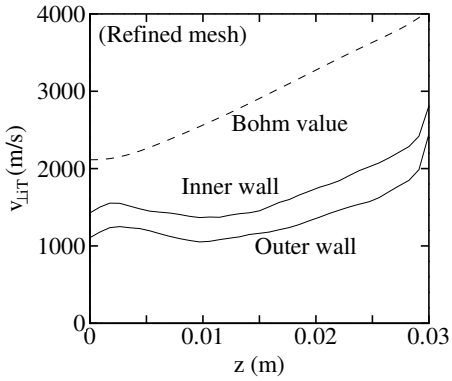

Figure 10. Ion perpendicular velocities at the domain boundaries and the Bohm velocity, for the refined mesh.

are significantly larger with the new mesh. These changes are related to a better resolution of the code near the boundaries, where gradients are larger, but the differences in the spatial profiles with the old mesh are not limited to thin regions near the boundaries. Furthermore, the new mesh corrects the strange profiles of ϕ and v_{ri} around the chamber mid-radius obtained with the old mesh.

Figure 9 plots axial profiles of different variables at the inner and outer boundaries using both meshes. The larger potential drops in the presheath with the new mesh lead to lower plasma densities at the domain boundaries, n_{eT}. The opposite trend was found for $v_{\perp iT}$ and the product of both, $j_{\perp iT} = en_{\perp eT}v_{\perp iT}$, turns out to increase with the new mesh. This is one of the main indications that the old mesh was computing incorrectly the ion radial fluxes. A larger $j_{\perp iT}$ means more wall recombination and thus larger neutral densities, n_{nT}, which finally is the required feedback to have a larger $j_{\perp iT}$. Also, the radial potential drop across half channel increases with ionization (Ahedo 2002a).

This comparison has demonstrated that the old mesh was too coarse to give acceptable radial structure of the plasma. The refined (and high-time consuming) mesh yields much more convincing results. In spite of these very positive results, Fig. 10 shows that the new mesh is still far from satisfying the Bohm condition on the radial velocities at the boundaries: the radial ion Mach number at the boundaries is about 0.5-0.6, compared to 0.2-0.3 in the old mesh. In terms of the radial kinetic energy, the figures are worse, since, with the new mesh, the ions have only about 30-40% of the required Bohm energy. If we consider that the execution time has been increased by 20 times and the high resolution of the new mesh, a Mach number of 0.6 is very disappointing.

6. CONCLUSIONS

An improved sheath model, which treats more correctly regions with high secondary electron emission, has been implemented in HPHall. This affects mainly the electron energy balance.

The fulfillment of the Bohm condition at the plasma-sheath transition has been shown to be a real and difficult problem to solve. The comparison of computations with two different meshes has demonstrated large differences in the radial structure of the plasma, which is more underveloped in coarse meshes. The resort to a virtual quasineutral layer between the computational domain and the sheath has proven to be incorrect.

In spite of the positive results obtained with the refined mesh, the radial ion velocity continues to be well below the Bohm value for a valid sheath transition. It is unclear to us whether an infinite mesh refining (without modifying any other algorithm in the PIC code) would lead to the fulfillment of the Bohm condition. But taking into account the alarming increment of the excution time and the moderate advance on fulfilling the Bohm condition, alternative ways of solving this issue must be found. To end, we want to emphasize that this is a central issue for the reliability of the simulation model since (i) the Bohm condition is unavoidable in a quasineutral-plus-sheath formulation and (ii) the radial plasma fluxes have a direct impact on the plasma global balances of currents and energies and the thruster performances.

ACKNOWLEDGMENTS

This research program is being carried out at the Universidad Politécnica of Madrid, with the financial support of the European Office of Aerospace Research and Development (Grant FA8655-04-1-3003). The original HPHall was developed at the Massachusetts Institute of Technology.

REFERENCES

Ahedo E., 2002a, Physics of Plasmas, 9, 3178

Ahedo E., 2002b, Physics of Plasmas, 9, 4340

Ahedo E., Gallardo J., Martínez-Sánchez M., 2003, Physics of Plasmas, 10, 3397

Fife J., Martínez-Sánchez M., 1995, In: 24th International Electric Propulsion Conference, Moscow, Russia, IEPC 95-240, Electric Rocket Propulsion Society, Cleveland, Ohio

Fife J., Martínez-Sánchez M., Szabo J., 1997, In: 33rd Joint Propulsion Conference, Seattle, WA, AIAA 97-3052, American Institute of Aeronautics and Astronautics,Washington, DC

Fife J.M., 1998, Hybrid-PIC Modeling and Electrostatic Probe Survey of Hall Thrusters, Ph.D. thesis, Massachusetts Institute of Technology

Hobbs G., Wesson J., 1967, Plasma Physics, 9, 85

Jolivet L., Roussel J.F., 2000, In: SP-465: 3rd Spacecraft Propulsion Conference, Cannes(Francia), 367–376, European Space Agency, Noordwijk, The Netherlands

Morozov A., 1991, Sov. J. Plasma Physics, 17, 393